Available online at www.sciencedirect.com
SCIENCE DIRECT®
Surface Science 519 (2002) 115–124
SURFACE SCIENCE
www.elsevier.com/locate/susc

Surface effects on angular distributions in X-ray-photoelectron spectroscopy

Y.F. Chen *

Department of Electrophysics, National Chiao Tung University, 1001 TA Hsueh Road, Hsinchu 30050, Taiwan, ROC

Received 8 February 2002; accepted for publication 8 May 2002

Abstract

The spatially varying inelastic mean free paths of photoelectrons emitted from a solid surface have been calculated from an extended Drude dielectric function, that considers the characteristic oscillator strength, damping constant, and critical-point energy for each subband of valence electrons. The results reveal that the additional inelastic scattering probability due to surface effects can be regarded as a surface excitation probability on the vacuum side and can be taken into account by use of a surface excitation parameter. The X-ray-photoelectron spectroscopy formalism in which elastic-scattering effects have been accounted for has been extended to include surface effects. The results show that surface effects lead to a reduction of photoelectron intensities at small emission angles and a sharp decrease at large angles (>75°) since surface excitations are most probable for glancing electrons. However, the difference between the results obtained with and without surface effects for emission angles less than 60° are small because of the method by which the results were normalized.

Keywords: X-ray photoelectron spectroscopy; Dielectric phenomena; Electron emission

1. Introduction

X-ray-photoelectron spectroscopy (XPS) is in frequent use for surface analysis [1–3]. Knowledge of photoelectron angular distribution is particularly important for quantitative analysis by angle-resolved XPS [4–6]. The usual formalism of XPS did not take into account the elastic-scattering effect. The influence of elastic-scattering on signal electron escape has attracted much attention of scientists since Baschenko and Nefedov [7] proved that elastic interactions might modify significantly the angular distribution of photoelectrons leaving a target. Theoretical methods to account for elastic-scatterings comprise Monte Carlo calculations [8–12] and analytical and numerical solutions of the transport equation [13–18]. Jablonski and Powell [5,9,12,19] have proposed that it is sufficient to modify the photoelectric cross-section with two correction factors, Q_x and β_{eff}, in order to account for elastic-scattering effects.

Recent studies on surface electron spectroscopy have revealed that surface effects are very important for the electrons of energies ranging from a few hundred to 2000 eV and especially for glancing escape electrons [20–28]. These results imply that

* Tel.: +886-35-712121x56106; fax: +886-35-729134.
E-mail address: yfchen@cc.nctu.edu.tw (Y.F. Chen).

0039-6028/02/$ - see front matter
PII: S0039-6028(02)02206-9

surface effects might also be important for the properties of photoelectron angular distributions. The surface effects result in spatial variation of the inelastic mean free path (IMFP). Applying the position-dependent IMFP in the Monte Carlo simulation, the influence of surface excitations on the angular distributions of photoelectron peak intensities has been investigated. The simulation results show that surface effects lead to a reduction of the intensities at small emission angles and a sharp decrease at large angles with respect to the surface normal. Although the Monte Carlo simulation is able to deal with the most complicated boundary conditions without considerable problems, a reliable and analytical approach can offer insight into practical analysis.

Dielectric response theory is often used to study the inelastic interaction of electrons near solid surfaces [20–30]. Previously, Yubero and coworkers [29,30] proposed a dielectric model to demonstrate the depth dependence of the IMFP. They show that there are interference effects between fields caused by the creation and movement of the electron as well as with the static core hole in the case of XPS. Therefore, The IMFP cannot be separated as bulk and surface contributions. Recently, we used dielectric response theory to derive the IMFP for electrons obliquely passing through a solid surface without consideration of interference effects [20,23]. It was found that the derived IMFP could be divided into well separated terms that can easily be calculated and interpreted. In contrast the previous expressions [29,30] are much more complex and not easy to handle in practice.

In this work, we first applied the Drude-like dielectric function [20–23] to study the characteristics of the spatially varying IMFP for an electron leaving the solid surface. It was found that the IMFP inside a solid can be considered as a constant equal to the bulk IMFP $\lambda_B(E)$ because the orthogonality of bulk and surface excitations compensates the surface excitation probability with a reduction of the bulk excitation probability [31]. On the other hand, the surface effects in the vacuum side result in additional energy-loss probability and may cause a significant influence on elastic-peak intensity. Therefore, the additional inelastic-scattering probability due to surface effects on the vacuum side of the interface can be considered as a surface excitation probability that can be conveniently described by the surface excitation parameter (SEP). By use of the SEP, the formalism of Jablonski and Powell [5,19] was extended to obtain a reliable and practical formalism so that the surface effects could be taken into account. The calculations reveal that the influence of surface excitations on the angular distribution was quite significant for glancing escape electrons. If normalization is performed at an emission angle of 54°44′ for the photoelectron signal intensity, the surface effects on the angular distribution are found to be somewhat diminished for emission angles less than 60°. Nevertheless, the calculated results with surface effects taken into account are in better agreement with the experimental data.

2. Differential inverse inelastic mean free path

The theoretical formula derived for an electron traveling in an infinite solid is usually used to describe inelastic interactions in surface electron spectroscopy. However, this formula does not consider surface effects intrinsic to the semi-infinite solid in the typical surface electron spectroscopy. Recently, we have derived the spatially varying differential inverse inelastic mean free path (DIMFP) for an electron with velocity $\boldsymbol{v}$ emitted from the solid surface which is chosen at the plane $z = 0$ with the z axis in the perpendicular direction from the solid with dielectric function $\varepsilon(\boldsymbol{q},\omega)$ to the vacuum. The spatially varying DIMFP for an escaping electron of energy $E = v^2/2$ to lose energy ω, $\mu(E \to E-\omega,\alpha,z)$, can be split up into bulk and surface terms [20,23],

$$\mu(E \to E-\omega,\alpha,z) = \mu_B(E \to E-\omega) + \mu_S(E \to E-\omega,\alpha,z), \quad (1)$$

where

$$\mu_B(E \to E-\omega) = \frac{1}{\pi^2 v}\int d^2Q \frac{|v_z|}{\tilde{\omega}^2 + (v_z Q)^2} \times \mathrm{Im}\left[-\frac{\Theta(-z)}{\varepsilon(\tilde{\boldsymbol{q}},\omega)}\right], \quad (2)$$

$$\mu_S(E \to E-\omega,\alpha,z) = \frac{1}{\pi^2 v}\int \mathrm{d}^2Q \frac{|v_z|}{\tilde{\omega}^2 + (v_z Q)^2} \times \mathrm{Im}[\Pi_S(\boldsymbol{v},z,\boldsymbol{Q},\omega)], \quad (3)$$

$$\Pi_S(\boldsymbol{v},z,\boldsymbol{Q},\omega) = \mathrm{e}^{-Q|z|}\left[\frac{\Theta(-z)}{\overline{\varepsilon}(z,\boldsymbol{Q},\omega)} - (2\cos(\tilde{\omega}z/v_z) - \mathrm{e}^{-Q|z|})\Theta(z)\right]\left[\frac{\varepsilon(\tilde{\boldsymbol{q}},\omega)^{-1}-1}{1+\overline{\varepsilon}(\boldsymbol{Q},\omega)^{-1}}\right], \quad (4)$$

$$\frac{1}{\overline{\varepsilon}(\boldsymbol{Q},\omega)} = \frac{Q}{\pi}\int_{-\infty}^{\infty}\frac{\mathrm{d}q_z}{q^2\varepsilon(\boldsymbol{q},\omega)}, \quad (5)$$

$$\frac{1}{\overline{\varepsilon}(z,\boldsymbol{Q},\omega)} = \frac{Q}{\pi}\int_{-\infty}^{\infty}\frac{\mathrm{d}q_z \mathrm{e}^{\mathrm{i}q_z z}}{q^2\varepsilon(q,\omega)}, \quad (6)$$

$\tilde{\omega} = \omega - v_\parallel \cdot Q$, $\tilde{q}^2 = Q^2 + \tilde{\omega}^2/v_z^2$, $\Theta(z)$ is the Heaviside step function, α is the electron emission angle with respect to the surface normal, and the notations $v = |\boldsymbol{v}|$, $\boldsymbol{q} = (\boldsymbol{Q}, q_z)$, $\boldsymbol{v} = (\boldsymbol{v}_\parallel, v_z)$, and $\boldsymbol{r} = (\boldsymbol{R}, z)$ are adopted, where $\boldsymbol{Q}$, $\boldsymbol{v}_\parallel$, and $\boldsymbol{R}$ represent the corresponding components parallel with the surface. Note that atomic units are used through this work, unless otherwise specified. Based on the conservation of energy and momentum the range of integration over $\boldsymbol{Q}$ is limited by

$$q_-^2 \leqslant \left(\frac{\tilde{\omega}}{v_z}\right)^2 + Q^2 \leqslant q_+^2, \quad (7)$$

where $q_\pm = \sqrt{2E} \pm \sqrt{2(E-\omega)}$. It can be seen that the bulk term which is independent of the position and emission angle, gives rise to the well known expression of the DIMFP of electrons moving in an infinite medium [31]. On the other hand, the spatially varying surface term is not confined to the interior of the solid, but also is responsible for inelastic scattering while the electron is at some distance outside the surface where all emitted electrons must travel.

Knowledge of the dielectric function $\varepsilon(\boldsymbol{q},\omega)$ is essential for studying the dependence of the DIMFP on electron energy, emission angle, and position. Although considerable progress has been achieved during the past decades in developing a quantum expression of the dielectric properties [32–34], the complex form prevents it from being put into practical electron spectroscopy applications. Therefore, a number of semiclassical dielectric models have been developed [20,35,36]. Previously, we have used Drude-like analytical functions to model the dielectric function. The real and imaginary parts of the dielectric function are given by [20–23]

$$\varepsilon_1(q,\omega) = \varepsilon_b - \sum_i \frac{A_i[\omega^2 - (\omega_i + q^2/2)^2]}{[\omega^2 - (\omega_i + q^2/2)^2]^2 + (\omega\gamma_i)^2} \quad (8)$$

and

$$\varepsilon_2(q,\omega) = \sum_i \frac{A_i\gamma_i\omega}{[\omega^2 - (\omega_i + q^2/2)^2]^2 + (\omega\gamma_i)^2}, \quad (9)$$

where A_i, γ_i and ω_i are, respectively, the oscillator strength, damping coefficient, and critical-point energy, associated with the ith interband transition. Note that we include a ε_b term to account for the background dielectric constant due to the influence of polarizable atomic cores [37]. The values of these parameters were determined by a fit of Eqs. (8) and (9), in the limit $q \to 0$, to the experimental optical data [38]. The internal consistency of the model dielectric function was assessed with two fundamental sum rules, the f-sum rule $\sum_i A_i = 4\pi N Z_v$ and another sum rule based on a limiting form of the Kramers–Kronig integral [37], where N is the number of atoms (or molecules) per unit volume and Z_v is the number of valence electrons per atom (or molecule). Table 1 lists the fiiting parameters for Cu, Ag, Au, Fe, Si, and GaAs solids. For Fe, Cu, Ag, and Au, our fits cover, respectively, the 3s + 3p, 3s + 3p, 4s + 4p, and 5s + 5p inner shells due to the strong overlaps of oscillator strengths between the valence band and these shells in the vicinity of their binding energies. It is worthwhile to mention that we use the bulk dielectric function $\varepsilon(\boldsymbol{q},\omega)$ to derive the DIMFP formula for the semi-infinite solid. This quasiclassical derivation is only exact for $Q = 0$. For $Q \neq 0$, Feibelman [39,40] has shown that the charge-density profile at the surface affects the properties of the surface response function, such as the surface-plasmon dispersion. However, the exact dependence of the dielectric function on

Table 1
Parameters in the model dielectric function of Eqs. (8) and (9) for several solids

Cu ($\varepsilon_b = 1.05$, $Z_v = 19$)			Ag ($\varepsilon_b = 1.01$, $Z_v = 19$)			Au ($\varepsilon_b = 1.00$, $Z_v = 19$)			Si ($\varepsilon_b = 1.06$, $Z_v = 4$)			GaAs ($\varepsilon_b = 1.03$, $Z_v = 8$)			Fe ($\varepsilon_b = 1.31$, $Z_v = 16$)		
A_i (eV^2)	γ_i (eV)	ω_i (eV)	A_i (eV^2)	γ_i (eV)	ω_i (eV)	A_i (eV^2)	γ_i (eV)	ω_i (eV)	A_i (eV^2)	γ_i (eV)	ω_i (eV)	A_i (eV^2)	γ_i (eV)	ω_i (eV)	A_i (eV^2)	γ_i (eV)	ω_i (eV)
64.0	0.03	0.00	160.0	0.05	0.00	79.0	0.1	0.00	8.0	0.12	3.42	2.08	0.10	2.92	40.0	0.12	0.00
6.0	0.30	0.30	4.0	0.80	4.80	9.0	1.0	3.10	15.0	0.35	3.52	25.97	0.61	3.16	30.0	2.00	0.45
6.5	0.65	2.50	30.0	2.20	5.30	36.0	1.9	4.10	45.0	0.66	3.80	3.90	1.20	3.84	50.0	4.00	1.50
5.5	0.70	3.10	40.0	8.00	6.00	17.0	2.3	5.30	82.8	0.50	4.25	58.80	0.70	4.60	130.0	6.00	3.20
4.0	0.70	3.70	220.0	9.00	14.00	60.0	4.0	8.17	5.0	2.42	4.55	17.00	0.35	4.90	10.0	2.00	6.04
55.0	2.60	5.05	120.0	4.38	22.50	100.00	9.0	12.00	32.0	1.10	5.34	10.00	1.00	5.60	41.4	4.80	9.56
42.0	4.76	8.93	150.0	10.00	31.30	120.0	10.0	14.00	52.0	3.40	6.40	43.44	2.42	6.70	28.0	3.20	12.90
172.0	10.18	14.74	310.0	36.00	40.00	155.0	6.0	21.30	15.0	5.00	9.40	10.00	6.50	9.80	300.0	18.00	20.00
80.0	8.00	25.60	200.0	20.0	45.00	145.0	7.2	29.50	15.0	6.50	14.0	32.00	7.00	12.50	60.0	30.00	48.00
240.0	32.00	40.00	100.0	12.00	55.00	280.0	20.0	38.50	6.0	5.00	18.4	10.00	3.50	21.50	190.0	10.00	58.00
90.0	30.00	55.00	200.0	15.00	68.00	360.0	28.0	63.00							993.0	100.00	84.00
85.0	30.00	65.00				183.0	26.0	100.00									
200.0	25.00	83.00															
500.0	65.00	120.00															
664.0	160.00	200.00															

momentum transfer is seldom known. Nevertheless, the expression adopted in Eqs. (6) and (7) for the q-dependence works correctly at the two ends of the momentum transfer, i.e. the optical end, $q \to 0$, and the Bethe ridge region, $q \to \infty$ [41]. Eq. (1) indicates that the range of integration over $\boldsymbol{Q}$ is rather large for electron energies larger than a few hundred eV, therefore the actual dispersion relation between the optical and the Bethe ridge region leads to only minor difference in the determination of the DIMFP [20–23].

With the model dielectric function, the DIMFPs have been calculated. Fig. 1 shows the position-dependence of the calculated DIMFPs for an 1 keV escaping electron with $\alpha = 0°$ inside Cu. It can be seen that the structures and peak positions of DIMFPs vary with the actual depth underneath the solid surface. Although surface excitations contribute largely at small energy losses as compared to bulk excitations, the spectral breadth arise from strong overlaps between the bulk and surface excitations. Slightly inside the solid, the DIMFP quickly approaches the result for electrons moving in the infinite solid, which indicates

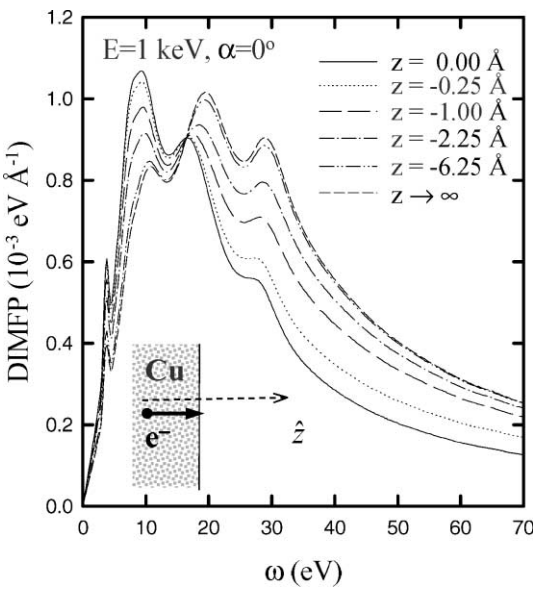

Fig. 1. Calculated results for the position-dependence of the calculated DIMFPs for an 1 keV escaping electron with $\alpha = 0°$ inside Cu.

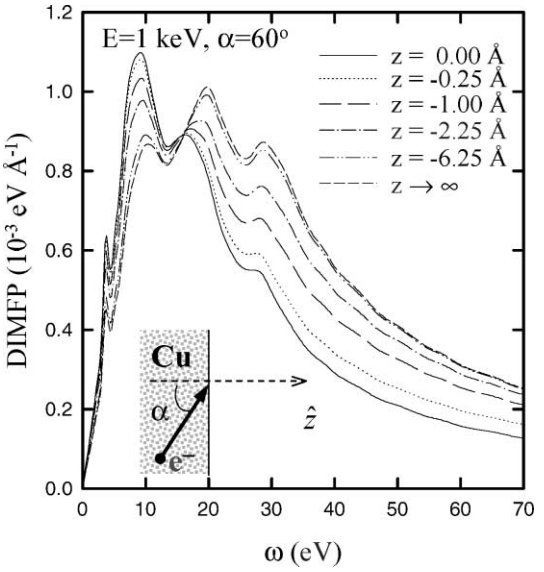

Fig. 2. Calculated results for the position-dependence of the calculated DIMFPs for an 1 keV escaping electron with $\alpha = 60°$ inside Cu.

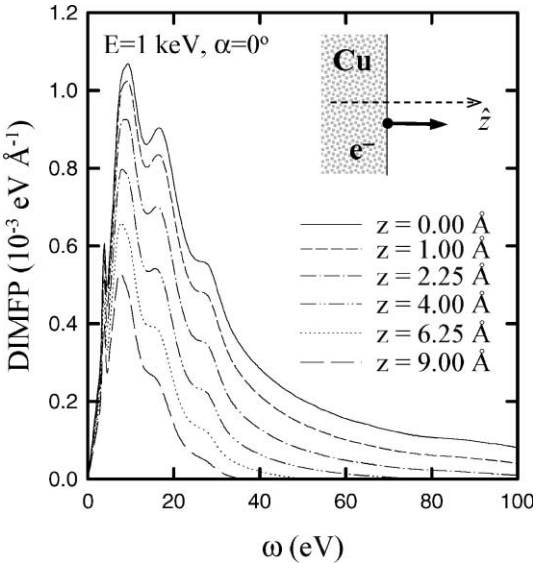

Fig. 3. Calculated results for the position-dependence of the calculated DIMFPs for an 1 keV escaping electron with $\alpha = 0°$ outside Cu.

that the surface effect is restricted to a limited region. Fig. 2 shows the position-dependence of the calculated DIMFPs for an 1 keV escaping electron with $\alpha = 60°$ inside Cu. In comparison with the result shown in Fig. 1 for $\alpha = 0°$, the small difference indicates that the angular-dependence of the DIMFP is rather weak in the solid.

Fig. 3 shows the position-dependence of the calculated DIMFPs for an 1 keV escaping electron with $\alpha = 0°$ outside Cu. The DIMFP on the vacuum side is found to get narrower and smaller at a larger distance from solid surface. It can be seen that surface effects occur over a rather limited distance range on the order of several Ångströms. Fig. 4 shows the position-dependence of the calculated DIMFPs for an 1 keV escaping electron with $\alpha = 60°$ outside Cu. Comparing with the result shown in Fig. 3 for $\alpha = 0°$, the angular-dependence of the DIMFP on the vacuum side is also rather weak. Further calculations for large emission angles show that the DIMFP can be regarded as angle-independent except for emission angles greater than 75°. The calculated results for an emission angle of $\alpha = 80°$ are depicted in Fig. 5. It can be seen that there are distinct differences in amplitude in comparison with the results shown in Figs. 3 and 4 for $\alpha \leqslant 60°$.

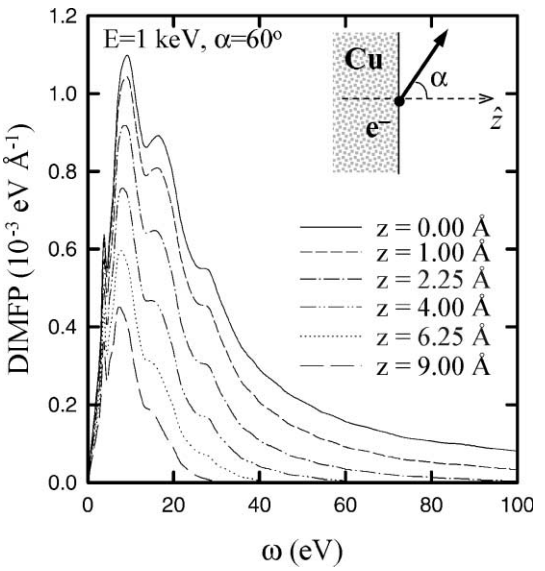

Fig. 4. Calculated results for the position-dependence of the calculated DIMFPs for an 1 keV escaping electron with $\alpha = 60°$ outside Cu.

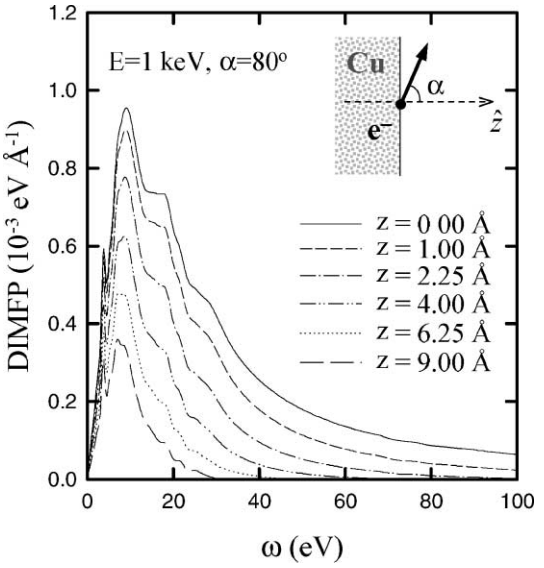

Fig. 5. Calculated results for the position-dependence of the calculated DIMFPs for an 1 keV escaping electron with $\alpha = 80°$ outside Cu.

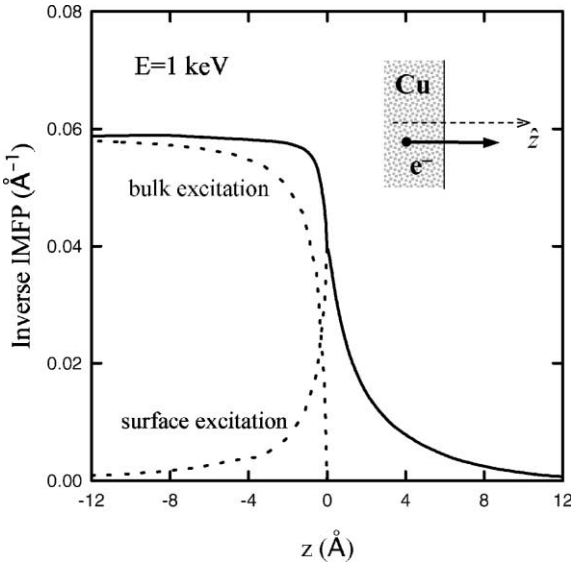

Fig. 6. A plot of the position-dependence of the calculated inverse IMFPs for an 1 keV electron leaving Cu.

3. Surface excitation parameter

The IMFP is the basic parameter for elastic-peak analysis in surface electron spectroscopy. The IMFP can be evaluated from an integration of DIMFP over ω:

$$\frac{1}{\lambda(E,\alpha,z)} = \int_0^E \mu(E \to E-\omega,\alpha,z)\,\mathrm{d}\omega. \tag{10}$$

Substituting Eq. (1) into Eq. (10), the spatially varing IMFP can be separated into a bulk and a surface terms,

$$\frac{1}{\lambda(E,\alpha,z)} = \frac{1}{\lambda_{\mathrm{B}}(E)} + \frac{1}{\lambda_{\mathrm{S}}(E,\alpha,z)}, \tag{11}$$

where $1/\lambda_{\mathrm{B}}(E) = \int_0^E \mu_{\mathrm{B}}(E \to E-\omega)\,\mathrm{d}\omega$ and $1/\lambda_{\mathrm{S}}(E,\alpha,z) = \int_0^E \mu_{\mathrm{S}}(E \to E-\omega,\alpha,z)\,\mathrm{d}\omega$.

Fig. 6 shows the position-dependence of the calculated inverse IMFPs for an 1 keV electron leaving Cu. To explore the surface effects, we also plot the inverse IMFPs for bulk and surface excitations inside Cu individually in Fig. 6. It can be seen that inside the solid an electron may experience surface excitations; however, the IMFP can be considered as a constant equal to the bulk IMFP $\lambda_{\mathrm{B}}(E)$ because the orthogonality of bulk and surface excitations compensates the surface excitation probability with a reduction of the bulk excitation probability [31]. On the other hand, the surface effects on the vacuum side result in additional energy-loss probability and may cause a significant influence on the elastic-peak intensity. Therefore, the IMFP can be practically approximated as

$$\lambda(E,\alpha,z) = \begin{cases} \lambda_{\mathrm{B}}(\mathrm{E}), & \text{inside the surface,} \\ \lambda_{\mathrm{S}}(E,\alpha,z), & \text{outside the surface,} \end{cases} \tag{12}$$

for electron energies greater than 100 eV and emission angles less than 75°. In other words, although the signal electrons may come from different depths, the additional inelastic scattering probability due to surface effects can be considered as surface excitation probability on the vacuum side. From the Poisson stochastic process, the probability for an electron leaving the solid surface to infinity without any surface excitations is given by

$$P_0(E,\alpha) = \exp\left[-\int_0^\infty \frac{1}{\lambda_{\mathrm{S}}(E,\alpha,z)}\,\frac{\mathrm{d}z}{\cos\alpha}\right]. \tag{13}$$

It appears practicable to introduce an integral parameter to characterize the surface effects:

$$P_S(E,\alpha) = \int_0^\infty \frac{1}{\lambda_S(E,\alpha,z)} \frac{dz}{\cos\alpha} = \int_0^E d\omega \int_0^\infty \mu_S(E \to E-\omega,\alpha,z) \frac{dz}{\cos\alpha}. \quad (14)$$

Physically, the SEP, $P_S(E,\alpha)$, represents the average number of surface excitation events experienced by an electron with energy E leaving the surface at an angle α [42]. Eq. (14) implies that the SEP will be proportional to the factor $1/\cos\alpha$ because there is practically no dependence of the DIMFP on the emission angle for $-75° < \alpha < 75°$. This angle-dependence of surface excitations has been verified experimentally [43]. In terms of the SEP, Eq. (13) can be written as $P_0(E,\alpha) = \exp[-P_S(E,\alpha)]$ for the probability of an electron leaving the solid surface without any surface excitations.

Applying $\varepsilon(\omega) = 1 - [\omega_p^2/(\omega^2 + i\gamma\omega)]$ with $\gamma \to 0$ into Eq. (3) and using Eq. (14), the SEP for the free-electron-gas dielectric function is given by

$$P_S^{FEG}(E,\alpha) = \frac{1}{\cos\alpha} \frac{2.896}{\sqrt{E}}, \quad (15)$$

where E is in units of electron-volts. The superscript "FEG" on the SEP refers to the free-electron-gas dielectric function. With the model dielectric function (Eqs. (8) and (9)), the SEPs have been calculated for some metals and semiconductors including Al, Cu, Ag, Au, Fe, Si, and GaAs. The calculation results reveal that the dependence of the SEP on electron energy and emission angle is nearly the same as for the free-electron-gas model. Namely, the SEP for metals and semiconductors can be conveniently fitted as

$$P_S(E,\alpha) = \frac{1}{\cos\alpha} \frac{a}{\sqrt{E}}, \quad (16)$$

where a is a fitting parameter. From the calculations, the parameter a is found to be 4.12, 2.45, 2.34, 3.06, 2.51, 2.50, and 2.15 for Al, Cu, Ag, Au, Fe, Si, and GaAs, respectively. Systematic deviations from Eq. (16) are generally within 5% for electron energies between 100 and 2000 eV and for emission angles less than 75°. A plot of SEP versus energy for electrons leaving Al, Au, Ag, Si, and GaAs is shown in Fig. 7. It can be seen that the energy-dependence in all cases is similar to that of the free-electron-gas model.

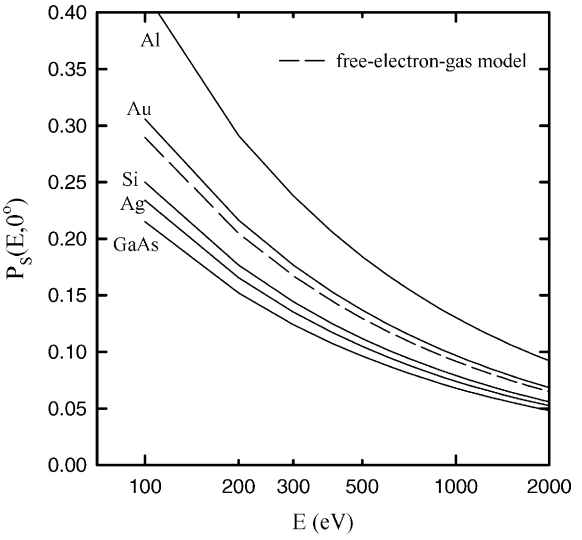

Fig. 7. A plot of SEP versus energy for electrons leaving Al, Au, Ag, Si, and GaAs. The dashed line indicates the result from the free-electron-gas model Eq. (15).

4. Angular distribution in XPS

If elastic-scattering and surface effects are neglected, the well-known formalism of XPS for the photoelectron signal intensity for a particular element and core level is given by [44]

$$I_x^0 = \Delta\Omega T D I_{ph} A_0 (d\sigma_x/d\Omega) \lambda_B M x, \quad (17)$$

where $\Delta\Omega$ is the acceptance solid angle of the analyzer, T is the transmission function of the analyzer, D is the detector efficiency, I_{ph} is the flux of incident X-rays, A_0 is the area of the sample at normal direction of the analyzer, $d\sigma_x/d\Omega$ is the differential photoelectric cross-section, M is the total density of atoms in the sample, and x is the fraction of atoms emitting photoelectrons for the element of interest. The superscript "0" on the photoelectron intensity refers to the neglect of elastic-scattering and surface effects. For unpolarized radiation and random orientation of atoms or molecules, the differential photoelectric cross-section is given by [45]

$$\frac{d\sigma_x}{d\Omega} = \frac{\sigma_x}{4\pi}\left[1 - \frac{\beta}{4}(3\cos^2\psi - 1)\right], \quad (18)$$

where σ_x is the total photoionization cross-section, ψ is the angle between the incident photons and emitted photoelectrons, and β is the asymmetry parameter.

Recently, Jablonski and Powell [5,9,12,19] reported that elastic-scattering effects in polycrystalline and amorphous solids can be taken into account by replacing $d\sigma_x/d\Omega$ in Eq. (18) with the following expression:

$$\left(\frac{d\sigma_x}{d\Omega}\right)_{el} = \frac{\sigma_x Q_x}{4\pi}\left[1 - \frac{\beta_{eff}}{4}(3\cos^2\psi - 1)\right], \quad (19)$$

where Q_x and β_{eff} are two correction parameters. Therefore, the XPS signal intensity is corrected as

$$I_x^{el} = \Delta\Omega T D I_{ph} A_0 (d\sigma_x/d\Omega)_{el} \lambda_B M x. \quad (20)$$

The superscript "el" indicates that elastic-scattering effects have been considered. Jablonski and Powell proposed that the two correction parameters could be conveniently approximated by the following simple expressions:

$$\beta_{eff} = a_1\cos^2\alpha + a_2\cos\alpha + a_3, \quad (21)$$

$$Q_x = b_1\cos^2\alpha + b_2\cos\alpha + b_3. \quad (22)$$

Values of the fitting parameters, a_i and b_i, are listed in Ref. [12] for each element, the principal photoelectron lines, and for Mg and Al X-ray source.

As mentioned in Section 2, the probability for an electron leaving the solid surface without any surface excitations can be written as $P_0(E,\alpha) = \exp[-P_S(E,\alpha)]$. To include surface effects on the XPS intensity, the modified formalism in Eq. (20) should be multiplied by the factor $\exp[-P_S(E,\alpha)]$. Therefore, the XPS signal intensity is finally corrected as

$$I_x^{els} = \exp[-P_S(E,\alpha)]\Delta\Omega T D I_{ph} A_0 (d\sigma_x/d\Omega)_{el} \lambda_B M x. \quad (23)$$

The superscript "els" denotes that both elastic-scattering and surface effects have been taken into account.

Previously, Jablonski and Zemek [46] reported a convenient experimental method for detemining the relative angular distribution of photoemission from solid materials. Recently, Hucek et al. [47]

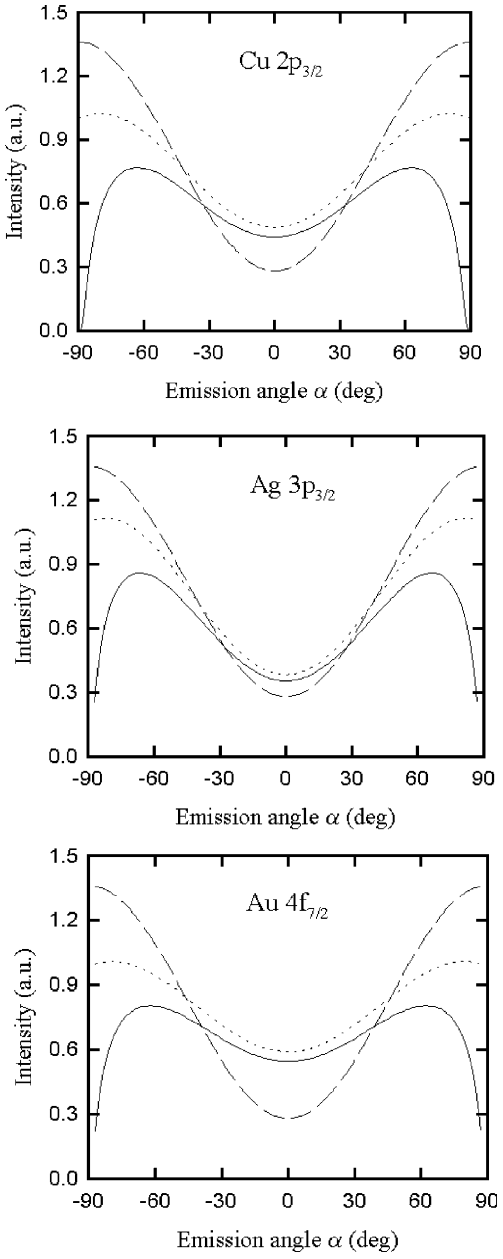

Fig. 8. Angular distributions of photoelectron signal intensities for several solids: (—) calculated results with Eq. (23); (···) calculated results with Eq. (20); (- - -) calculated results with Eq. (17). (a) $Cu2p_{3/2}$ photoelectrons, (b) $Ag3p_{3/2}$ photoelectrons, (c) $Au4f_{7/2}$ photoelectrons.

reported a new series of angle-resolved XPS experiments. According to their experimental setup, the angle between the X-rays and the direction of analysis is ψ, and is related to α by $\psi = 180° - \alpha$.

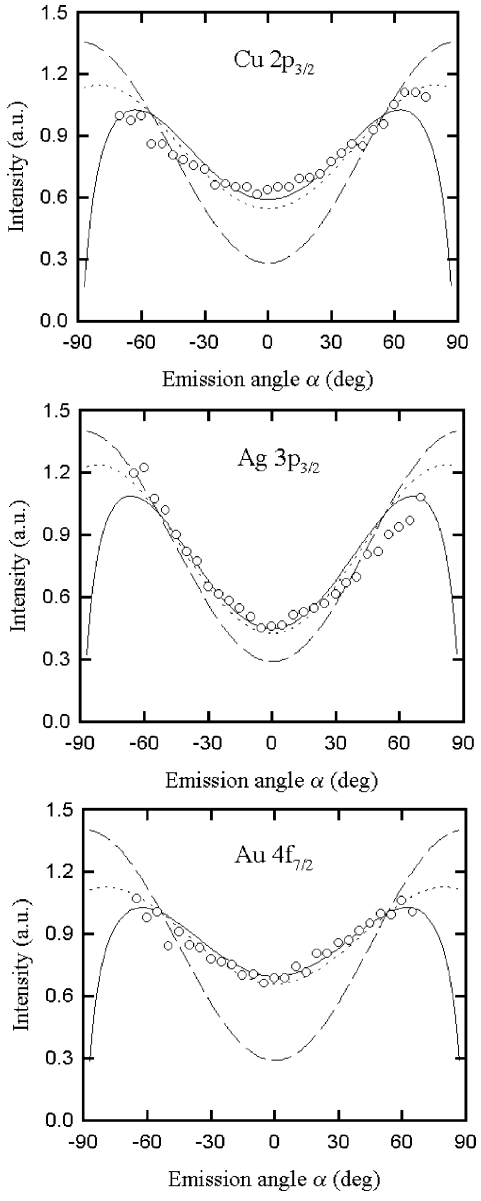

Fig. 9. Angular distributions of photoelectron signal intensities normalized with respect to the emission angle $\alpha = 54°44'$ for several solids: (—) calculated results with Eq. (23); (···) calculated results with Eq. (20); (- - -) calculated results with Eq. (17); (○) experimental data [44]. (a) $Cu2p_{3/2}$ photoelectrons, (b) $Ag3p_{3/2}$ photoelectrons, (c) $Au4f_{7/2}$ photoelectrons.

Using Eqs. (16) and (23), we have calculated angular distributions for the of $Cu2p_{3/2}$, $Ag3p_{3/2}$, and $Au4f_{7/2}$ photoelectron lines excited by Al Kα radiation. Fig. 8(a)–(c) show these angular distributions calculated with (solid lines) and without (dotted lines) surface effects. It can be seen that the additional energy-loss probability due to surface effects results in a reduction of the signal intensities calculated with consideration of elastic-scattering effects. Comparison with the intensities expected from the straight line approximation (dashed lines), in which elastic-scattering and surface effects are neglected, shows that the anisotropy in the angular-dependence of the photoelectron intensities is always decreased by elastic-scattering for $-60° < \alpha < 60°$. On the other hand, surface effects result in a sharp decrease of the photoelectron intensities at large angles. This result is due to the fact that surface excitations are most probable for glancing electrons, as expected from Eq. (16).

Fig. 9 compares the experimental data of $Cu2p_{3/2}$, $Ag3p_{3/2}$, and $Au4f_{7/2}$ lines excited by Al Kα radiation with the theoretical calculations from Eqs. (17), (20) and (23). Note that all results are normalized so that they are identical at the magic angle ($\alpha = 54°44'$). It is seen that the surface effects on the angular distribution are diminished in large part in the range of $-60° < \alpha < 60°$ because of the normalization. This may be the reason why the previous formalism [5,19] (without consideration of surface effects) compares well with the experimental data [46–48]. Nevertheless, the influence of surface excitations is still significant at larger emission angles due to the increased surface excitation probability at these angles; more experiments are needed in the future to provide an extensive experimental base for developing a reliable formalism.

5. Conclusion

A theoretical model based on an improved dielectric function was used to calculate the position-dependent IMFP for an electron emitted from a solid surface. The results indicate that inside the solid the IMFP can be regarded as a constant equal to the IMFP value for bulk excitations,

whereas the surface effects on the vacuum side can be characterized by a SEP. SEP results for Al, Cu, Ag, Au, Fe, Si, and GaAs have been fitted to an analytical equation $(1/\cos\alpha)(a/\sqrt{E})$ with a single fitting parameter a. Using this analytical expression, the formalism of Jablonski and Powell [5,19] was practically modified to account for surface effects. The corrected results showed that surface effects lead to a reduction of the intensities at small emission angles and a sharp decrease at large angles since surface excitations are most probable for glancing electrons. It was also found that surface effects on the angular distribution in XPS lead to reduced intensities. Consideration of surface effects, however, leads to better agreement with the experimental data overall.

References

[1] D.P. Woodruff, T.A. Delchar, Modern Techniques of Surface Science, Cambridge University Press, New York, 1986.
[2] J.C. Riviere, Surface Analytical Techniques, Clarendon, Oxford, 1990.
[3] S. Tougaard, Surf. Interface Anal. 8 (1986) 257.
[4] J.E. Fulghum, Surf. Interface Anal 20 (1993) 161.
[5] A. Jablonski, C.J. Powell, Phys. Rev. B 50 (1994) 4739.
[6] W.H. Gries, J. Vac. Sci. Technol. A 13 (1995) 1304.
[7] O.A. Baschenko, V.I. Nefedov, J. Electron. Spectrosc. Relat. Phenom. 17 (1979) 405.
[8] H. Ebel, M.F. Ebel, A. Jablonski, J. Electron. Spectrosc. Relat. Phenom. 35 (1985) 155.
[9] A. Jablonski, Surf. Interface Anal. 14 (1989) 659.
[10] W.S.M. Werner, Surf. Interface Anal. 18 (1992) 217.
[11] H. Yoshikawa, T. Tsukamoto, R. Shimizu, V. Crist, Surf. Interface Anal. 18 (1992) 757.
[12] A. Jablonski, Surf. Interface Anal. 23 (1995) 29.
[13] A.L. Tofterup, Phys. Rev. B 32 (1985) 2808.
[14] V.M. Dwyer, J.A.D. Matthew, Surf. Sci. 193 (1988) 549.
[15] R. Bindi, H. Lanteri, P. Rostaing, Surf. Sci. 197 (1988) 295.
[16] I.S. Tilinin, W.S.M. Werner, Phys. Rev. B 46 (1992) 13739.
[17] W.S.M. Werner, I.S. Tilinin, M. Hayek, Phys. Rev. B 50 (1994) 4819.
[18] A. Jablonski, I.S. Tilinin, J. Electron. Spectrosc. Relat. Phenom. 74 (1995) 207.
[19] A. Jablonski, C.J. Powell, Surf. Interface Anal. 20 (1993) 771.
[20] Y.F. Chen, Y.T. Chen, Phys. Rev. B 53 (1996) 4980.
[21] Y.F. Chen, P. Su, C.M. Kwei, C.J. Tung, Phys. Rev. B 50 (1994) 17547.
[22] Y.F. Chen, J. Vac. Sci. Technol.A. 13 (1995) 2665.
[23] Y.F. Chen, Surf. Sci. 345 (1996) 213.
[24] S. Tougaard, Phys. Rev. B 34 (1986) 6779.
[25] D.D. Hawn, B.M. De Koven, Surf. Interface Anal. 10 (1987) 63.
[26] S. Tougaard, J. Kraaer, Phys. Rev. B 43 (1991) 1651.
[27] F. Yubero, S. Tougaard, Phys. Rev. B 46 (1992) 2486.
[28] H. Yoshikawa, R. Shimizu, Z.J. Ding, Surf. Sci. 261 (1992) 403.
[29] F. Yubero, S. Tougaard, Surf. Interface Anal. 19 (1992) 269.
[30] A. Cohen Simonsen, F. Yubero, S. Tougaard, Phys. Rev. 56 (1997) 1612.
[31] R.H. Ritchie, Phys. Rev. 106 (1957) 874.
[32] P.A. Fedders, Phys. Rev. 153 (1967) 438.
[33] D.E. Beck, Phys. Rev. B 4 (1971) 1555.
[34] J.F. Dobson, G.H. Harris, J. Phys. C 20 (1987) 6127.
[35] R.H. Ritchie, A.L. Marusak, Surf. Sci. 4 (1966) 234.
[36] V. Nazarov, Phys. Rev. B 49 (1994) 10663.
[37] D.Y. Smith, E. Shiles, Phys. Rev. B 17 (1978) 4689.
[38] E.D. Palik (Ed.), Handbook of Optical Constants of Solids, Academic Press, New York, 1985.
[39] P.J. Feibelman, Prog. Surf. Sci. 12 (1982) 287.
[40] P.J. Feibelman, Phys. Rev. B 9 (1974) 5077.
[41] R.H. Ritchie, R.N. Hamm, J.E. Turner, H.A. Wright, W.E. Bolch, in: W.A. Glass, M.N. Varma (Eds.), Physical and Chemical Mechanisms in Molecular Radiation Biology, Plenum Press, New York, 1991, p. 99.
[42] R.F. Egerton, Electron Energy-Loss Spectroscopy in the Electron Microscope, Plenum Press, New York, 1986.
[43] C.J. Powell, Phys. Rev. 175 (1968) 511.
[44] C.S. Fadley, R.J. Baird, W. Siekhaus, T. Novakov, A.A.L. Bergstrom, J. Electron. Spectrosc. Relat. Phenom. 4 (1974) 93.
[45] R.F. Reilman, A. Msezane, S.T. Manson, J. Electron. Spectrosc. Relat. Phenom. 8 (1976) 389.
[46] A. Jablonski, J. Zemek, Phys. Rev. B 48 (1993) 4799.
[47] S. Hucek, I.S. Tilinin, J. Zemek, J. Electron. Spectrosc. Relat. Phenom. 85 (1997) 263.
[48] O.A. Baschenko, G.V. Machavariani, V.I. Nefedov, J. Electron. Spectrosc. Relat. Phenom. 34 (1984) 305.